Journal of Electrochemical Science and Technology
Vol. 3, No. 3, 2012, 123-134
http://dx.doi.org/10.5229/JECST.2012.3.3.123

Journal of Electrochemical Science and Technology

Evaluation of Tolerance of Some Elemental Impurities on Performance of Pb-Ca-Sn Positive Pole Grids of Lead-Acid Batteries

H.A. Abd El-Rahman†, A.G. Gad-Allah, S.A. Salih, and A. M. Abd El-Wahab
Chemistry Department, Faculty of Science, Cairo University, 12613 Giza, EGYPT

ABSTRACT :

The electrochemical performance of positive pole grids of lead-acid batteries made of Pb-0.08%Ca-1.1%Sn alloys without and with 0.1 wt% of each of Cu, As or Sb and with 0.1 wt% of Cu, As and Sb combined was investigated by electrochemical methods in 4.0 M H_2SO_4. The corrodibility of alloys under open-circuit conditions and constant current charging of the positive pole, the positive pole gassing and the self-discharge of the charged positive pole were studied. All impurities (Cu, As, Sb) were found to decrease the corrosion resistance, R_{corr} after 1/2 hour corrosion, but after 24 hours an improvement in R_{corr} was recorded for Sb containing alloy and the alloy with the three impurities combined. While an individual impurity was found to enhance oxygen evolution reaction, the impurities combined significantly inhibition this reaction and the related water loss problem was improved. Impedance results were found helpful in identification of the species involved in the charging/discharging and the self-discharge of the positive pole. Impurities individually or combined were found to increase the self-discharge during polarization (33-68%), where Sb containing alloy was the worst and impurities combined alloy was the least. The corrosion of the positive pole grid in the constant current charging was found to increase in the presence of impurities by 5-10%. Under open-circuit, the self-discharge of the charged positive grids was found to increase significantly (92-212%) in the presence of impurities, with Sb-containing alloy was the worst. The important result of the study is that the harmful effect of the studied impurities combined was not additive but sometimes lesser than any individual impurity.

Keywords: Positive pole; Pb-Ca-Sn alloys; Lead-acid batteries; recycled Lead

Received August 22, 2012 : Accepted September 12, 2012

1. Introduction

Most lead used in the manufacture of grids is provided by the recycling process of lead batteries and other lead products.[1-3] Tolerance of elemental impurities in pig lead for the manufacture of grids is based on industrial standards, such as, ASTM Designation B29-79(84) and Battery Council International (BCI). According to these standard, maximum tolerance levels of some elements As, Cu and Sb are at less than 20 ppm. From the environmental and economical points of view, it is encouraging to use lead produced in the recycling process with the minimal additions of pure lead. Lead-Calcium grids dominate value-regulated lead-acid batteries (VRLAB) market for use in cars due to their superior self-discharge performance, low water problems and long shelf-time.[4-7] Addition of Sn in the grid alloys is effective in recovery after overcharging, on long standing and in improving the corrosion resistance.[8-10] Typical composition of Pb-Ca-Sn alloys is 0.08-0.12% Ca and 0.2-0.4% Sn for negative grids while as positive grids 0.04-0.06% Ca and 1.0-1.2% Sn is used.[11] Research studies to improve the performance of Pb-Ca-Sn grids by controlling the alloying elements and heat treatments received atten-

†Corresponding author. Tel.: +202-35676565
E-mail address: abdelrahman_hamid@hotmail.com

tion.[12-17]

The present work is a preliminary evaluation study that is aimed to encourage the use of the recycled lead with impurity levels considerably above those in the industrial standards. The selected elements, namely, antimony, arsenic and copper are some of the potential impurities from recycling of lead-acid batteries based on Pb-Sb grids and Pb-Cu alloys used in many industrial applications. These elements are expected to deteriorate the electrochemical performance and corrosion resistance of positive pole made from Pb-Ca-Sn alloys. The corrosion behavior, the positive pole gassing and the self-discharge problems of positive pole grids made of the commercial alloy Pb-0.08% Ca-1.1% Sn with 0.1 wt% additions of Cu, As and Sb individually and combined were investigated in 4.0 M H_2SO_4.

2. Experimental

Disc working electrodes were cut from rods of cast Pb-Ca-Sn alloys with the compositions given in Table 1. 2 cm long rod of the alloy was coated with a thin epoxy adhesive (Araldite®, Ciba, Switzerland) and inserted in thick-walled glass tubing with appropriate cross-sectional area. Cross sectional area of the alloy, ca. 0.28 cm^2, was only left to contact the test solution. A stout copper rode was screwed from the other end of the alloy rod to provide the electrical contact of the electrode. The electrodes were mechanically polished with successive grades of emery papers up to 1200 grit, then washed with acetone, double distilled water and finally with a fine tissue so that the surface appeared bright and free from defect. A three-electrode cell was employed in all electrochemical tests. The counter electrode was a platinum sheet of area ca. 2×2 cm^2 and positioned in the cell to face the working disc electrode. The potential of the alloy electrode was measured versus an Hg/Hg_2SO_4/1.0 M H_2SO_4 reference electrode (0.680 V vs. SHE). All potentials are given relative to the previously mentioned reference electrode. Chemically ultra-pure sulfuric acid 98% stock was used for preparation of solutions by appropriate dilution using doubly distilled water. All measurements were conducted in unstirred naturally aerated 4.0 M H_2SO_4 acid solutions at a constant temperature of 25±0.2°C.

The different electrochemical measurements were carried using the electrochemical system IM6 Zahner electric, Meßtechink, Germany. The electrode capacitance, C (F) and resistance, R (Ω) values were extracted from the impedance, Z (Ω), and the phase shift angle, θ values of the cell at a frequency, f, of 1.0 kHz; $Z = (R^2 + (1/2\ \pi fC)^2)^{1/2}$ and $\tan\theta = 1/2\ \pi fRC$. With the large counter electrode used, the cell impedance was reduced to that of the working electrode and the solution resistance between the working and counter electrodes. Impedance spectra were recorded at the respective corrosion potential of the alloy in the frequency range 0.1 Hz-100 kHz using an ac potential of 3 mV peak to peak. The experimental impedance spectra were fitted with the appropriate equivalent circuits using the "SIM" program included with the IM6 package. The suitability of the elements in the proposed equivalent circuits to fit the experimental data was judged by the error% of the fitting and by comparing the calculated and the experimental impedance plots. Potentiodynamic tests were carried out by holding the respective alloy electrode at 2.0 V versus the Hg/Hg_2SO_4/1.0 M H_2SO_4 reference electrode for 15 minutes before scanning the potential to 1.2 V at a scan rate 10 mV/s. Constant current charging/discharging of the alloy electrode was done by applying a cathodic current of 0.54 mA cm^{-2} for 5 minutes to remove any reducible species from the alloy surface, then the current polarity was reversed to oxidize the alloy for 60 minutes. Finally, the current polarity was again reversed to reduce the formed PbO_2 on the alloy surface. The reduction continued until the H_2 evolution. The potential of the alloy electrode was followed

Table 1. Composition of Pb-Ca-Sn alloys used in the study.

Alloy	Description	Composition%
A	No impurity added	Sn 1.1214, Sb 0.00033, Cu 0.00034, As 0.00019, Ca 0.08279, Pb 98.7807
A-As	With 0.1 wt% As	Sn 1.146, Sb 0.00035, Cu 0.00033, As 0.0982, Ca 0.08151, Pb 98.674
A-Cu	With 0.1 wt% Cu	Sn 1.1234, Sb 0.00021, Cu 0.098, As 0.00018, Ca 0.08279, Pb 98.681
A-Sb	With 0.1 wt% Sb	Sn 1.1146, Sb 0.1021, Cu 0.0934, As 0.1021, Ca 0.08166, Pb 98.704
A-ACS	With 0.1 wt% As + 0.1 wt% Cu + 0.1 wt% Sb	Sn 1.1369, Sb 0.00031, Cu 0.00034, As 0.00026, Ca 0.08093, Pb 98.409

with time during all the stages of the constant current charging/discharging. In the self-discharge tests, the alloys were anodized at 0.54 mA cm^{-2} for 30 minutes before opening the circuit and recording open-circuit potential and impedance until the alloys were fully self-discharged.

3. Results and Discussion

3.1. Corrosion behavior under open-circuit conditions

Under open circuit conditions, passive $PbSO_4$ films were naturally formed on the tested alloys as a result of the thermodynamically favorable reaction of Pb component in the alloy with H_2SO_4. The reaction was completed by reducing H^+ to H_2 gas and/or reduction of O_2. The passive $PbSO_4$ layer is the main corrosion product of the alloys.

The effect of impurities on the general corrosion of the alloy in 4.0 M H_2SO_4 (the typical sulfuric acid concentration for most fully charged lead-acid cells) was tested after 1/2 hour (as usually employed in electrochemical corrosion testing of metals) and after 24 h hours (for deeper evaluation) using the non-destructive electrochemical impedance spectroscopy (EIS).

Fig. 1 shows Nyquist plots for the five alloys taken at the corrosion potential, E_{corr}, after 1/2 hour and 24 hours. The shape of the impedance plots at low frequencies (at higher values of real and imaginary parts of impedance, Z_{re} & Z_{im}) is determined by the diffusion impedance and the impedance of the passive film at 1/2 hour corrosion, while the passive film resistance dominates the behavior after corrosion for 24 hours. It is known that linear Z_{re}-Z_{im} parts, at lower frequencies, are attributed to the Warburg diffusion impedance while the distorted semi-circles are attributed to the presence of insulating layers on the corroding alloy (more explanation will be given later). Corrosion resistance, R_{corr}, of the alloy is masked by the previously mentioned properties and cannot directly be inferred from the distorted semi-circles at high frequencies. Proposed equivalent circuits that represent structure and electrode kinetics of the alloy/solution interface in this study are shown in Fig. 2. Model 1 is a

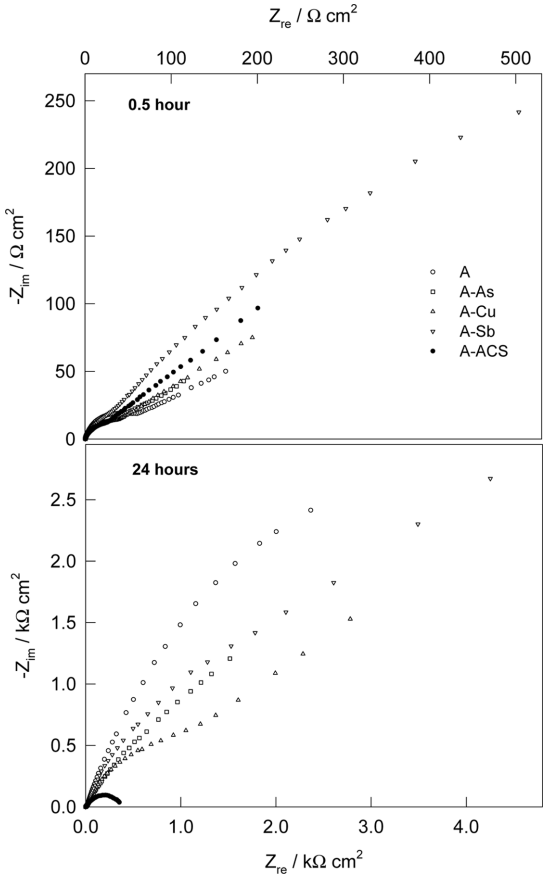

Fig. 1. Nyquist plots for Pb-Ca-Sn alloys without and with different impurities after 1/2 hour (Upper) and 24 hours (Lower) corrosion in 4.0 M H_2SO_4.

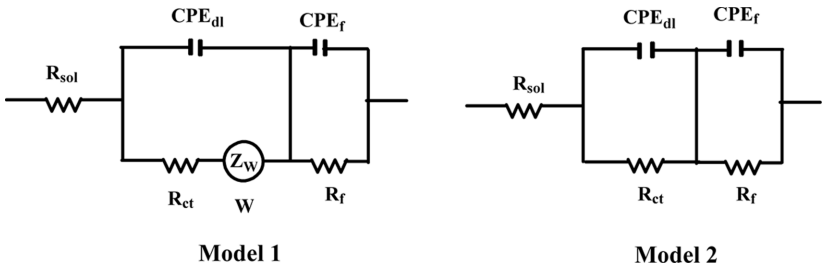

Fig. 2. Equivalent circuits used to simulate the impedance spectra for corrosion of Pb-Ca-Sn alloy in 4.0 M H_2SO_4. For definition of each component in the circuits see text.

serial connection that include 3 parts: 1- Passive film properties (as a parallel combination of film resistance, R_f, and capacitance, C_f), 2- Capacitive and faradaic processes of the interface (as a parallel combination of double layer capacitance, C_{dl}, and the two faradaic contributions; charge transfer resistance, R_{ct}, and Warburg diffusion impedance, Z_w) and 3- Solution resistance, R_{sol}. C_{dl} and C_f are represented by constant phase elements, CPE_{dl} and CPE_f to account for the surface heterogeneity, distribution of surface properties and imperfect dielectric material, respectively.[18,19] The capacitive reactant, $Z_{im,\phi}$, of a constant phase element, CPE, is given by:

$$Z_{im,\phi} = \frac{1}{\omega_0 C(j\omega/\omega_0)^{\phi}} \quad (1)$$

Where $\omega = 2\pi f$, $\omega_o = 2\pi f_0$, f and f_0 are the working frequency and a reference one to keep the dimensions of capacitance C, $j = -1^{1/2}$ and the exponent ϕ takes a value between 0 and 1, $\phi =$ for conventional capacitance. R_{ct} is identified as R_{corr} in the present study. Model 2 is Model 1 but without the diffusion impedance contribution. Other equivalent circuits that described the corrosion behavior of lead alloys in H_2SO_4[7,19-22] were tested and found inappropriate for fitting of the experimental data in the present work, whereas Model 1 was found successful in other studies.[23,24]

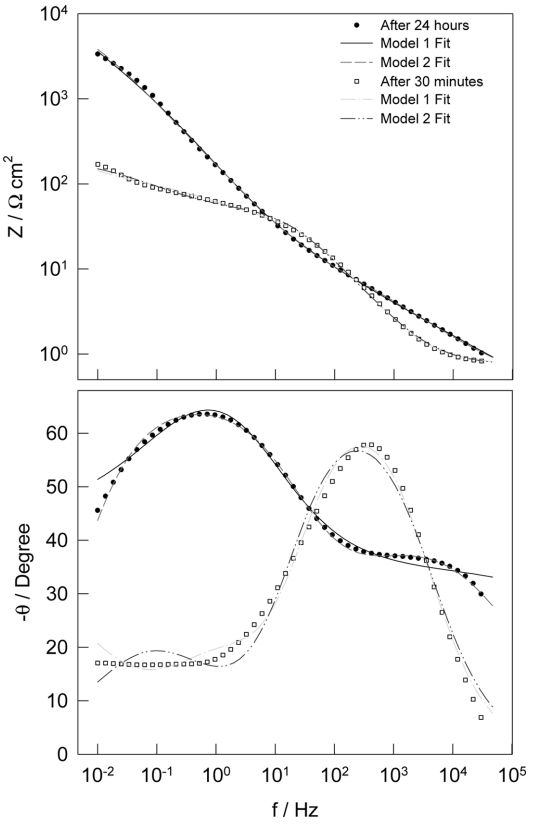

Fig. 3. Bode plots for Pb-Ca-Sn alloy after 1/2 hour and 24 hours corrosion in 4.0 M H_2SO_4. The lines are the simulations of the experimental data according to Model 1 and Model 2 shown in Fig. 2.

Fig. 3 shows Bode plots for the fitting of the experimental data of alloy A after 1/2 hour and 24 hours corrosion with proposed Models 1 & 2. Bode plots allow better and uniform estimation of the fitting quality over the entire frequency range studied. While Model 2 is clearly better than Model 1 for fitting the 24 hours data, Model 1 fits slightly better than Model 2 the 1/2 hour data. The deterioration of the fitting quality at 1/2 hour with both models compared to that at 24 hours is attributed the quasi-stationary nature of the interface at the beginning of the corrosion rather than the assumed stationary state required to access data in EIS technique. The key fitting parameters are given in Table 2 and represented graphically as a function of the alloy composition in Fig. 4. Generally, R_{corr} values after 1/2 hour are higher than after 24 hours, probably due to an increase in the surface roughness (area) of the corroding alloy. The alloy with the three impurities combined (A-ACS) shows the least decrease in R_{corr} with increasing the corrosion time, indicating the fast attainment of steady state of corrosion for this alloy. After 1/2 hour, the presence of the impurities individually or combined causes a decrease in R_{corr} in the order: A-ACS > A-As > A-Sb > A-Cu. However, after 24 hours, alloys A-Sb & A-ACS have higher R_{corr} than alloy A while the other two alloys have lower R_{corr} values. The improvement of corrosion resistance after 24 hours for alloys A-Sb and A-ACS is attributed to thickening of a barrier passive film that is rich in Sb species and composed mainly of $PbSO_4$. Both Cu and As impurities seem to have a deteriorating effect on the insulating properties of the passive film after 24 hours of corrosion. The resistance of the naturally formed passive $PbSO_4$ film, R_f, is represented on logarithmic scale to facilitate comparison and it increases substantially with corrosion time for all alloys due to thickening of the insulating $PbSO_4$ film.[25,26] From Table 2, both R_f and the parameter of the diffusion

Table 2. Key fitting parameters for impedance spectra of Pb-Ca-Sn alloys without and with different impurities in 4.0 M H_2SO_4 at the corrosion potential. Models 1 & 2 were used to fit the experimental data after 1/2 h and 24 hours, respectively. The models were shown in Fig. 3.

Corrosion time	Parameter	A	A-As	A-Cu	A-Sb	A-ACS
1/2 hour						
	$R_{ct}/\Omega\ cm^2$	35.0	15.3	23.9	22.5	15.2
	$W/\Omega\ cm^2\ s^{-1/2}$	16.6	15.8	31.8	67.62	28.0
	$C_{dl}/\mu F\ cm^{-2}$	311.61	398.96	246.82	252.53	208.54
	$R_f/\Omega\ cm^2$	53.9	44.0	56.8	198.3	54.3
	$C_f/\mu F\ cm^{-2}$	358.57	333.14	388.93	257.68	362.5
24 hours						
	$R_{ct}/\Omega\ cm^2$	8.9	7.1	6.0	11.0	14.8
	$C_{dl}/\mu F\ cm^{-2}$	39.36	41.36	34.37	24.24	102/36
	$R_f/k\Omega\ cm^2$	8.9	4.5	2.7	5.2	0.5
	$C_f/\mu F\ cm^{-2}$	162.79	74.25	74.86	102.86	99.25

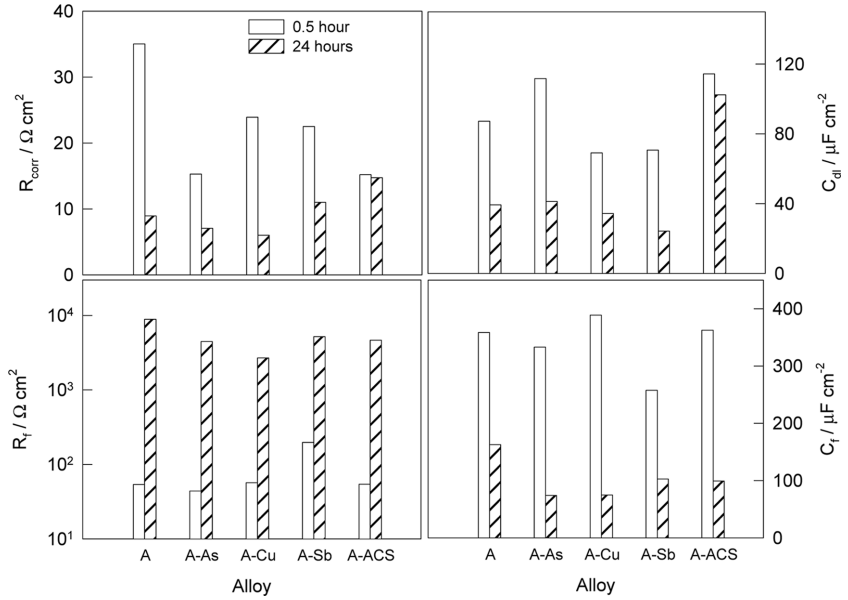

Fig. 4. Dependence of the corrosion resistance, R_{corr}, the passive film resistance, R_f, the double layer capacitance, C_{dl}, and the passive film capacitance, C_f, on the composition of the Pb-Ca-Sn alloy and the corrosion time in 4.0 M H_2SO_4.

impedance W follow the same order: A-Sb > A-Cu > A-ACS > A > A-As. Since W is inversely proportional to the diffusion coefficient(s) of the species involved in the alloy corrosion,[27] one can inferred that after 1/2 hour, the presence of Sb, Cu and three impurities combined retard the diffusion while the presence of As enhance the diffusion. The substantial increase in R_f with the concurrent decrease in R_{corr} after 24 hours indicate that the passive film is defective and does not inhibit the transport of the corrosive species. The thickening of $PbSO_4$ film is supported by the pronounced decrease in C_f after 24 hours, compared to that after 1/2 hour for all alloys. This is because $PbSO_4$ is considered an imperfect dielectric material; the increase in its thickness is expected to decrease capacitance according to equation of the parallel plate condenser. The fact that $PbSO_4$ film is an imperfect dielectric is supported by the experimental value of ϕ (0.6-0.7), where a perfect dielectric should have $\phi = 1$. The increase in the $PbSO_4$ surface coverage with the corrosion time is inferred from the slighter decrease in C_{dl}.

3.2. Oxygen evolution kinetics on positive grids

Anodic polarization curves of the alloys at potential more positive than 1.0 V have two concurrent faradaic contributions; PbO_2 formation and oxygen evolution reaction (OER). Current due the PbO_2 formation process must be subtracted (or greatly suppressed) to obtain pure current due to OER. A simple procedure was followed in the present study to suppress PbO_2 formation. The alloy potential was held at sufficiently high anodic potential of 2.0 V for sufficient time to observe excessive gassing (15 minutes). The total anodic charge, Q_t, was determined from the respective i-time curves by integration. A following potentiodynamic scan from 2.0 V to –0.2 V was performed at a scan rate10 mV/s. The E-i data in the potential range 1.4-1.8 V were used to construct Tafel plots for OER. The parts of the potentiodynamic curves for the reduction of PbO_2 to Pb^{2+} species at peak C1 [19,22,23,28] is showed in Fig. 5. The charge of peak C1, Q_{C1}, is a measure of the amount of PbO_2 formed at 2.0V for 15 minutes. The efficiency percentage of PbO_2 formation, $E_{PbO_2}\%$, was calculated according to the relation:

$$E_{PbO_2}\% = \left(\frac{2Q_{C1}}{Q_t}\right) \times 100 \qquad (2)$$

Inset of Fig. 5 shows that $E_{PbO_2}\%$ values are very low ($E_{PbO_2}\% < 0.25\%$). Q_{C1} may be underestimated due to the self-discharge of PbO_2 via the chemical disproportionation reaction with the underlying Pb layers [21,25,26]. However, the current contribution of PbO_2 formation may be neglected and the anodic current is safely attributed to OER from 2.0 V down to 1.4.

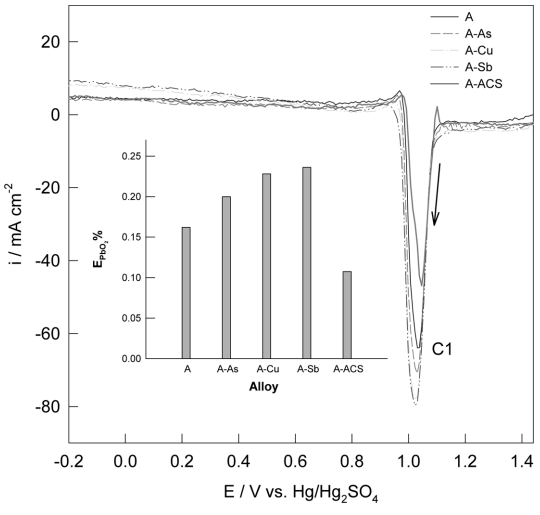

Fig. 5. Potentiodynamic curves for reduction of PbO_2 film formed on Pb-Ca-Sn alloys without and with different impurities in 4.0 M H_2SO_4 at a scan rate 10 mV/s. Alloys were pre-oxidized at 2.0 V for 15 minutes. Inset) versus alloy type.

Fig. 6 shows Tafel plots constructed from potentiodynamic curves recorded according to the previously mentioned procedure. As can be seen in Fig. 6, linear Tafel plots over about two orders of magnitudes of current density were obtained for all alloys. The nearly independence of Tafel slope (b_a = 0.15 mV) on the alloy composition signifies the same mechanism for OER on all alloys. Apparently, any individual impurity enhances OER but impurities combined significantly inhibit OER. The percentage inhibition of OER current, $I_{O_2}\%$, at E = 1.7 V was calculated according to the relation:

$$I_{O_2}\% = \left(1 - \frac{I_{O_2,\,impurity}}{I_{O_2,\,A}}\right)_{E\,=\,1.7V} - 100 \qquad (3)$$

Where and were the current densities of OER on alloy with an impurity and on alloy A, respectively. Inset of Fig. 6 shows that a weak negative inhibition (speed up) of OER occurs and follows the order: A-Cu > A-As > A-Sb. A stronger positive inhibition of OER occurs for alloy A-ACS. Thus, positive pole grids made of alloy A-ACS, in the constant potential

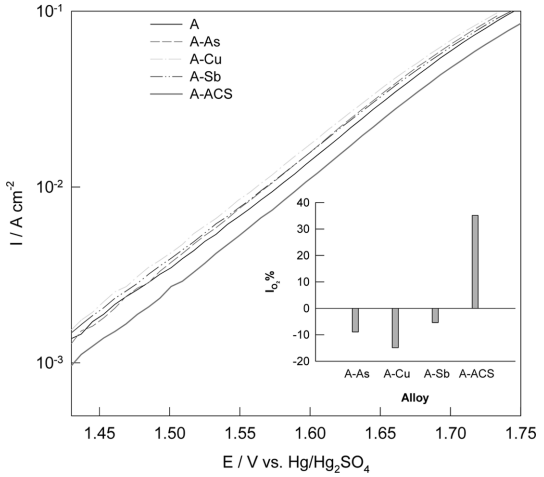

Fig. 6. Anodic polarization curves for the oxygen evolution reaction on Pb-Ca-Sn alloys without and with different impurities in 4.0 M H_2SO_4. Inset) versus alloy type.

charging, is superior in reduction of gassing (i.e., water loss due to OER) than the pure alloy A.

3.3. Galvanostatic charging/discharging of positive grids

Each alloy was cathodically polarization at 0.54 mA cm^{-2} for 5 minutes in 4.0 M H_2SO_4 to remove any reducible species on the surface, especially the transformation of the naturally formed passive $PbSO_4$ to Pb. Then the polarity was reversed to charge the positive pole and the oxidation was continued for 60 minutes. Finally, the polarity was again reversed to discharge and the reduction continued until H_2 evolution dominated and all reducible species in the surface were reduced.

Fig. 7 illustrates the instantaneous variation in potential, E, capacitance, C, and resistance, R, during the oxidation (charging)/reduction (discharging) cycle of alloy A. C is represented on the logarithmic scale to show uniformly the large change in properties of the alloy/solution interface. The fact that the time of reduction (~80 min.) is higher than the oxidation time (60 min.) indicates that new reducible species are involved in the reduction, beside the oxidation products. These new species are mainly Pb atoms in the surface layer of alloy beneath the PbO_2 layer, beside O_2 produced in the oxidation and O_2 already present in the naturally aerated H_2SO_4. Three oxidation regions a-c can be distinguished:

- The potential arrest a (at −0.95 V) is close to the equilibrium potential of the redox $Pb/PbSO_4$ in 4.0 M H_2SO_4.[29] It is attributed to the growth of $PbSO_4$ film, and it lasts for 8 minutes. The corresponding C decreases to a minimum and then it increases slowly. The corresponding R increases with time to a quasi-stationary value by the end of this region, indicating the growth of a thin $PbSO_4$ film.

- A following sharp increase in E from −0.95 to 1.52 V occurs in region b. In this region, a sharp decrease in C to a minimum and a sharp increase in R to a maximum occur, due to the formation of a highly insulating inner PbO film beneath the $PbSO_4$ layer.[21,22,28,30] The compact $PbSO_4$ film is assumed to retard the diffusion of H_2SO_4 through the barrier film and consequently, pH value increases at the alloy/$PbSO_4$ interface and the formation of PbO becomes favorable.

- In region c, E decreases slowly from 1.52 V to 1.29 V (up to 38 minutes) and then it starts to increase slowly up to 1.34 V due to OER. Concurrently, C starts to increase very sharply and R decreases to the solution resistance. This indicates the transformation of PbO to the conducting PbO_2 and growth of PbO_2 from the underlying Pb as well. It is noted that C increases more slowly after 38 minutes and continues to increase even during the initial period of reduction after reversing the current polarity (region d). The increase in C is attributed to a change in the dielectric properties of PbO_2 layer as a result of the concurrent OER[21] and involvement of O_2 species in the growing PbO_2 layer.

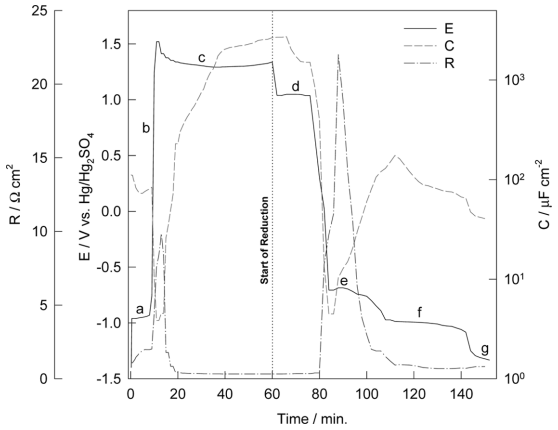

Fig. 7. Instantaneous potential, E, capacitance, C, and resistance, R, during galvanostatic oxidation/reduction of alloy A at 0.54 mA cm^{-2} in 4.0 M H_2SO_4.

Reduction of PbO_2 occurs in three two-electron steps d-f:

- The potential arrest d (at 1.05 V) is close to the equilibrium potential of the redox $PbSO_4/PbO_2$ in 4.0 M H_2SO_4 and attributed to the electo-reduction of PbO_2 to $PbSO_4$ according to the process:[21,29]

$$PbO_2 + 4H^+ + SO_4^{2-} + 2e \rightarrow PbSO_4 + 2H_2O \qquad (4)$$

Arrest d lasts for 16 minutes. In the first 6 minutes of this arrest, C increases to a maximum and then it deceases substantially during the next 14 minutes. Meanwhile R stays low during arrest d. C and R behaviors can be explained as follows: At the beginning, the high electrical conductivity of PbO_2 facilitates electron transfer through the film and the reduction occurs partially at PbO_2/alloy interface and through all parts of PbO_2 film. Concurrently, O_2 molecules formed in the oxidation are gradually removed

from the film by both, electro-reduction and by physical diffusion. After 6 minutes of reduction, the passive layer at film/alloy interface is completed and further reduction of PbO_2 to $PbSO_4$ can only result in thickening of the passive layer.

- E shows a rapid transition from 1.0 V to –0.7 V (~6 minutes) to region e where the reduction of basic lead sulphates (namely, $PbO{\cdot}PbSO_4$ and $3PbO{\cdot}PbSO_4$) to Pb are assumed.[21,29] In the transition d → e, a substantial decrease in C and a corresponding sharp increase in R occur due to the formation of PbO beneath $PbSO_4$ layer. This is possible due to the rise of pH value in the inner layer of $PbSO_4$ and the electro-reduction of the remaining PbO_2 to PbO occurs according to the process:[21]

$$PbO_2 + 2H^+ + 2e \rightarrow PbO + H_2O \qquad (5)$$

The equilibrium potential of the above process is ~0.4 V. Thus, the final stage of PbO_2 electro-reduction involves the formation of the highly insulating PbO layer at alloy/film interface. In the middle of region e, C starts to increase and R decrease due to the electro-reduction of PbO to the conducting Pb.

- In region f, $PbSO_4$ is reduced to Pb[21,29] with a noticeable, but slow, decrease in C. The capacitance behavior in this region reflects two effects: a decrease in $PbSO_4$ surface coverage and an increase in the interfacial acid concentration.

- At the end of region f, E shifts to a more negative potential (~−1.3 V) where H_2 evolves in region g. In this region, there is a decrease in C and a slight increase in R, probably due to the H_2 bubbles formed on the alloy surface.

It should be mentioned that the amount of the charge consumed in the reduction of PbO_2 to Pb^{2+} is significantly less than half of the total anodic charge. This is attributed to the self-discharge of PbO_2 with the underlying lead according to the disproportionation reaction:[29,31,32]

$$PbO_2 + Pb + 2H_2SO_4 \rightarrow 2PbSO_4 + 2H_2O \qquad (6)$$

The charge density lost in the self-discharge, Q_{SD}, is given by:

$$Q_{SD} = 0.5(Q^r_{basicPbSO_4} + Q^r_{PbSO_4} - Q^r_{PbO_2}) \qquad (7)$$

Where $Q^r_{PbO_2}$, $Q^r_{basicPbSO_4}$ and $Q^r_{PbSO_4}$ are charge densities of reduction of PbO_2 to Pb^{2+}, basic $PbSO_4$ (namely, $PbO{\cdot}PbSO_4$ and $3PbO{\cdot}PbSO_4$) and $PbSO_4$, respectively. The factor 0.5 in the above Eq. (5) was used to account for the extra reduction charge of Pb^{2+} species produced from the underlying Pb as a result of its reaction with PbO_2 according to equation (6). The charge consumed in formation of PbO_2 $Q^f_{PbO_2}$ is given by:

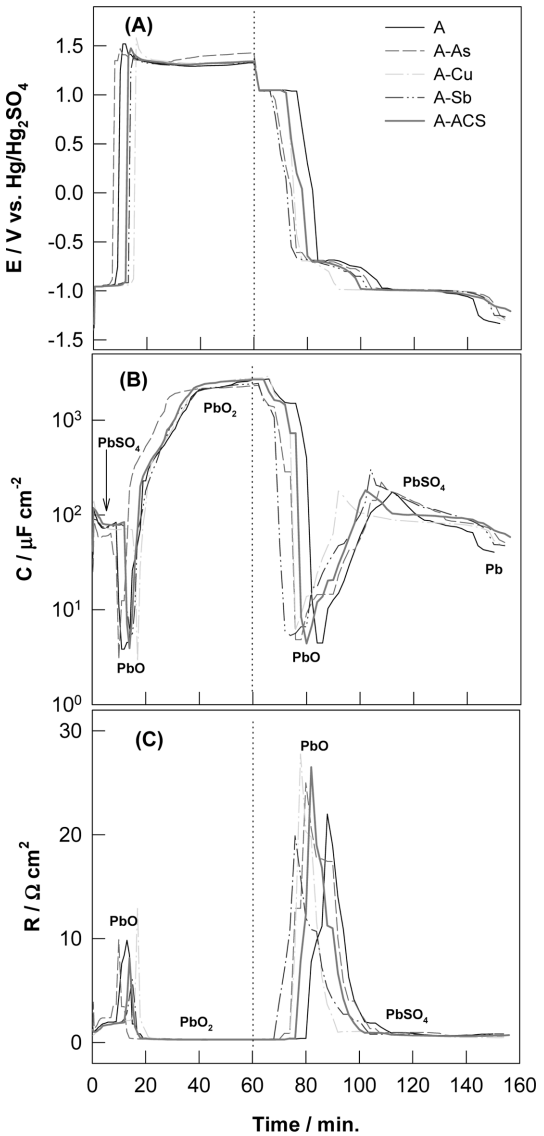

Fig. 8. Instantaneous potential (A), capacitance (B) and resistance (C) during galvanostatic oxidation/reduction of Pb-Ca-Sn alloys without and with different impurities at 0.54 mA cm^{-2} in 4.0 M H_2SO_4. The predominating species are shown on curves of parts (A) & (B).

Table 3. Charge consumed in the redox processes of interest in the charging/discharging of Pb-Ca-Sn alloys at 0.54 mA cm^{-2} in 4 M H_2SO_4.

Charge	A	A-As	A-Cu	A-Sb	A-ACS
$Q^r_{PbO_2}$/C cm^{-2}	0.497	0.346	0.346	0.259	0.410
$Q^r_{PbOPbSO_4}$/C cm^{-2}	0.518	0.605	0.303	0.626	0.432
$Q^r_{PbSO_4}$/C cm^{-2}	0.734	0.972	1.188	0.994	1.080
$Q^r_{PbO_2}$/C cm^{-2}	1.75	1.92	1.84	1.88	1.92
Q_{SD}/C cm^{-2}	0.378	0.616	0.573	0.681	0.551
A_{corr}/mg cm^{-2}	0.94	1.03	0.99	1.01	1.03
SD_P%	21.6	32.1	31.1	36.2	28.7

$$Q^f_{PbO_2} = 2(Q^r_{PbO_2} + Q_{SD}) \quad (8)$$

The positive pole corrosion, A_{corr} (g cm^{-2}) in terms of the Pb mass loss in the form of PbO_2 was calculated from $Q^r_{PbO_2}$ according to Faraday's laws:

$$A_{corr} = \frac{Q^r_{PbO_2} \times 207.19}{4F} \quad (9)$$

The value 207.19 g/atom is the atomic mass of Pb and F is the Faraday constant, 96500 C/equivalent. It should be noted that the positive pole corrosion is different from the general corrosion of the alloy in part 3.1. This is because the former corrosion form occurs as a result of charging of the positive pole, while the latter corrosion form occurs naturally under open-circuit conditions. The percentage of the self-discharge under polarization, SD_P%, is given by:

$$SD_P\% = (Q_{SD}/0.5Q^f_{PbO_2}) \times 100 \quad (10)$$

Fig. 8 shows the effect of impurities on the charging/discharging behavior of E, C and R. Curves of all alloys show the same features. Lead species that dominate C & R behaviors are given in the figure. Due to the exceptionally high resistivity of PbO, the growth of PbO layer beneath $PbSO_4$ outer layer and its disappearance appear in Fig. 8 as two sets of C and R peaks. The initial set corresponds to the transformation $Pb \rightarrow PbO \rightarrow PbO_2$. The second set signifies the transformation $PbO_2 \rightarrow PbO \rightarrow Pb$. The time needed for appearance of C or R peak of the initial set follows the order: A-As < A < A-ACS < A-Sb < A-Cu. This time is proportional to charge needed for the completion of $PbSO_4$ layer and the increase in pH beneath it to the level that the formation of an inner PbO layer becomes favorable. The results indicates that Cu and Sb impurities delayed the formation of PbO while As speeded up it. The time of the second set follows the order: A-Sb < A-Cu < A-AS < A-ACS < A, and it indicates that the impurities speed up the formation of PbO from PbO_2. The amount of the charge consumed in the redox processes of interest, beside A_{corr} and SD_P%, are given in Table 3. Fig. 9 shows the effect of impurities on the positive pole corrosion and the self-discharge under polarization compared to alloy A, expressed as the relative percentage of the positive pole corrosion, RA_{corr}% and the relative percentage of the self-discharge, RSD_P%. As can be seen, RA_{corr}% increases in the order: A-Cu < A-Sb < A-As = A-ACS. RSD_P% increases the order: A-ACS < A-Cu < A-As < A-Sb. The effect of impurities on the

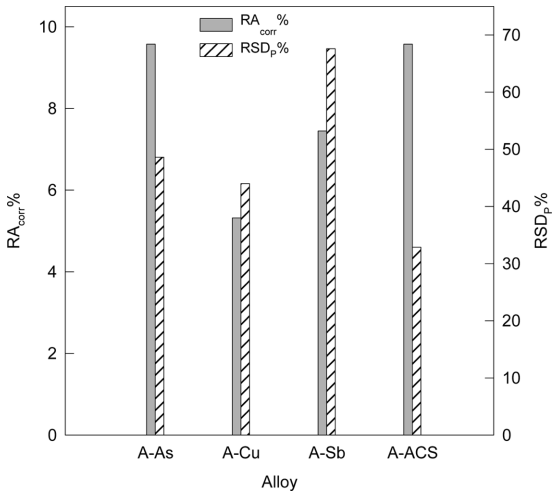

Fig. 9. Dependence of the percentages of the relative positive pole corrosion, RA_{corr}%, and the relative self-discharge under polarization, RSD_P%, on alloy type.

deterioration of the self-discharge under polarization (33-68%) is more pronounced than on the positive pole corrosion (5-10%). The alloy containing the three impurities combined (A-ACS) is the lowest in RSD_P% while Sb-alloy is the highest. On the repetition of the charging/discharging, more penetration of the alloy surface, due to the self-discharge, becomes the predominant factor in the deterioration of the mechanical properties and the chemical stability of the positive pole grid.

3.4. Self-discharge of positive grids

Fig. 10 shows the instantaneous variations in the open-circuit potential, E_{oc}, C and R of the pre-oxidized (pre-charged) alloys in 4 M H_2SO_4. Alloys were anodized (charged) at 0.54 mA cm^{-2} for 30 minutes and then the circuit was opened and the alloys were allowed to fully self-discharge under open-circuit conditions. The most probable stoichiometric redox processes are given on the E_{oc}-time curves. According to the potential curves, the full self-discharge corresponds to the disproportionation of PbO_2 with the underlying Pb to the final product $PbSO_4$. During the self-discharge there were substantial changes in C and R due to the generation of compounds, such as, PbO, basic $PbSO_4$ and $PbSO_4$, which have considerably different dielectric and insulating properties from the conducting PbO_2. At the beginning, E_{oc} stays at ~1.2 V for 2-3 minutes. Then, it shifts rapidly to more or less stable potential at ~1.07 V for a period of time that depends on the alloy type. Thereafter, E_{oc} decays rapidly to several consecutive ill-definite potential arrests. The probable redox processes involved in the potential arrests are shown on the potential curves in Fig. 10. Concurrently, C increases initially to maximum (~1 mF) an then decreases rapidly to a very low values (~2-4 μF). It is assumed that the self-discharging of PbO_2 starts and with time the acidity at the alloy/film interface decreases and PbO formation starts. R stays low for most of the initial period but starts to increase sharply with the PbO formation. The minimum capacitance, C_{min}, and maximum resistance, R_{max}, indicate the maximum amount of PbO. It should be mentioned that C_{min} and R_{max} for alloys A and A-ACS occur at longer times (50 & 60 minutes) than the rest of alloys with an individual impurity (11-18 minutes), indicating the slower formation and growth of the inner insulating layer of PbO for alloys A and A-ACS. The final stage of the self-discharge is characterized by a further but slower E_{oc} decay with a noticeable irregular increase in C and a decrease in R. Such changes are associated with the chemical transformation of the inner PbO to $PbSO_4$. After ~3 hours, E_{oc} records practically the same value for all alloys and corresponds to

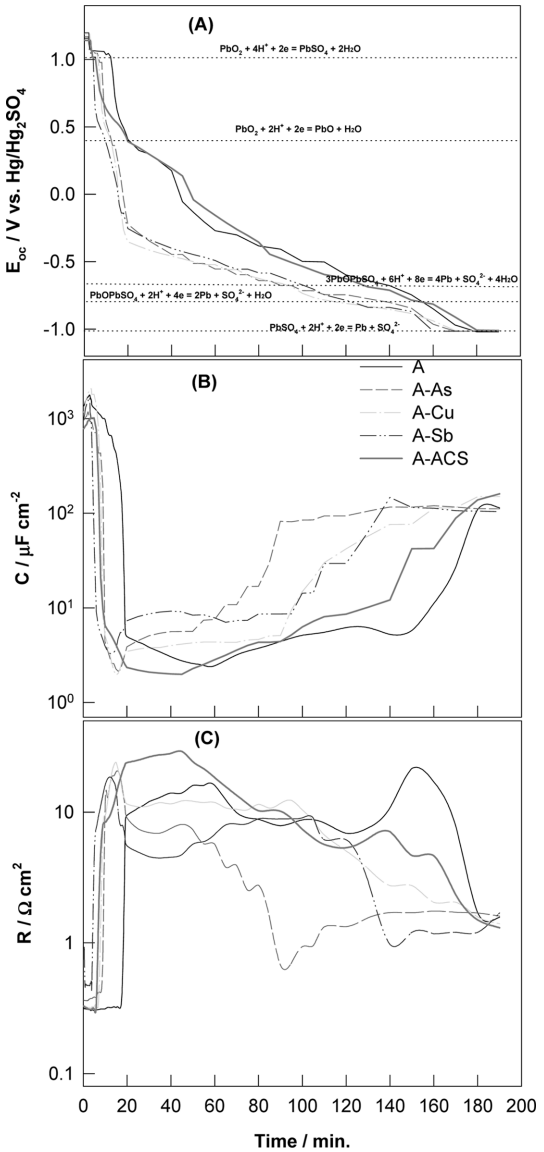

Fig. 10. Instantaneous open-circuit potential, E_{oc} (A), capacitance (B) and resistance (C) during the self-discharge of Pb-Ca-Sn alloys without and with different impurities in 4.0 M H_2SO_4. The electrodes were pre-oxidized at 0.54 mA cm^{-2} for 30 minutes. The various redox processes involved during the self-discharge are shown on E_{oc}-time curves.

the potential of the redox $Pb/PbSO_4$. Also, C and R become very close for all alloys.

The effect of impurity type on the self-discharge was estimated from Fig. 10, in terms of the reciprocal of time period before the fall of E_{oc} under 1 V, $1/t_{SD}$. The value $1/t_{SD}$ was taken as a measure for the rate of the self-discharge under open-circuit conditions. The results show that $1/t_{SD}$ increases in the order: A < A-As < A-Cu < A-ACS < A-Sb. Thus, alloys with impurities have higher self-discharge rate than the alloy without impurity. The fact that Sb-alloy has the highest rate of self-discharge is consistent with the known harmful effect of Sb on the self-discharge of positive pole grids of antimonial lead alloys.[4,5] The percentage of the relative increase in $1/t_{SD}$ for alloys with impurities compared to alloy A is: A-As 92%, A-Cu 108%, A-ACS 127%, A-Sb 212%.

Conclusion

- Corrosion behavior showed a strong dependence on the corrosion period. After 1/2 hour corrosion, impurities (Cu, As, Sb) individually or combined were found to decrease the corrosion resistance, R_{corr}. After 24 hours, R_{corr} for A-Sb and A-ACS alloys was found to be higher than the alloy A (without any impurity).

- Any individual impurity was found to enhance oxygen evolution reaction, but the impurities combined significantly inhibited the reaction.

- The inner insulating PbO formation and transformations were identified as peaks in the resistance and capacitance measurements.

- In the constant current charging of the positive pole, impurities were found to increase both the corrosion of the positive pole grid (5-10%) and the self-discharge of PbO_2 under discharge conditions (33-68%). The alloy A-Sb was the worst in the self-discharge of the charged positive pole while alloy A-ACS was the least.

- The self-discharge of the charged positive grids under open-circuit conditions was found to increase significantly (92-212%) in the presence of impurities, with alloy A-Sb was the worst.

References

1. Stevenson, M., *Recycling|Lead-Acid Batteries*: *overview*, in *Encyclopedia of Electrochemical Power Sources*, J. Garche, ed., Elsevier (2009).
2. S. Prolich and D. Sewig, *J. Power Sources*, **57**, 27 (1995).
3. T. W. Ellis and A. H. Mirza, *J. Power Sources*, **195**, 4525 (2010).
4. D. Pavlov, *Lead-Acid Batteries, Science and Technology*, Ch. 1, Elsevier (2011).
5. D. A. Rand, P. T. Moseley, J. Garche and C. D. Parker, Eds., *Valve-Regulated Lead-Acid Batteries*, Ch. 2, Elsevier (2004).
6. R. D. Perngaman, *J. Power Sources*, **33**, 13 (1991).
7. W. R. Osorio, L. C. Peixoto and A. Garcia, *J. Power Sources*, **195**, 1726 (2010).
8. C. S. Lakshmi, J. E. Manders and D. M. Rice, *J. Power Sources*, **73**, 23 (1998).
9. G. Bourguignon, A. Maitre E. Rocca, J. Steinmetz and L. Torcheux, *J. Power Sources*, **113**, 301 (2003).
10. E. Rocca and J. Steinmetz, *Electrochim. Acta*, **44**, 4611 (1999).
11. V. F. Bashev, N. E. Zhitnik, V. A. Ivanov, D. A.Rybalka and Yu. A. Tkackenko, *Metalloy*, **1**, 85 (2011).
12. E. Rocca , G. Bourguignon and J. Steinmetz, *J. Power Sources*, **161**, 666 (2006).
13. H. Li, W.X. Guo, H. Y. Chen, D. E. Finlow, H. W. Zhou, C. L. Dou, G. M. Xiao, S. G. Peng and W. W. Wei, H. Wang, *J. Power Sources*, **191**, 111 (2009).
14. W. Zhang, A. Li, H. Chen, B. Lan, K. Pan, T. Zhang, M. Fang, S. Liu and W. Zhang, *J. power Sources*, **203**, 145 (2012).
15. W. Wang, B. Zhou, G. S. Rohrer , H. Guo and Z. Cai, *Material Science and Engineering: A*, **527**, 3695 (2010).
16. F. A. Pérez-González, C. G. Camurri, C.A. Carrasco and R. Colás, *Materials Characterization*, **64**, 62 (2012).
17. H. Li, W. X. Guo, H. Y. Chen, D. E. Finlow, H. W. Zhou, C. L. Dou, G. M. Xiao, S. G. Peng, W. W. Wei and H. Wang, *J. Power Sources*, **191**, 111 (2009).
18. J. R. MacDonald, *J. Electroanal.Chem.*, **223**, 25 (1987).
19. S. Brinic, M. Metikos-Hukovic and R. Babic, *J. Power Sources*, **5**, 19 (1995).
20. M. M. Burashnikova, I. A. Kazarinov and I. V. Zotova, *J. Power Sources*, **207**, 19 (2012).
21. H. A. Abd El-Rahman, S. A. Salih and A. M. Abd El-Wahab, *Mat. -wiss u. werkstofftech.*, **42**, 784 (2011).
22. M. Metikos-Hukovic, R. Babic and S. Brinic, *J. Power Sources*, **157**, 563 (2006).
23. P. Simon, N. Bui, N. Pebere, F. Dabosi and L. Albert, *J. Power Sources*, **55**, 63 (1995).
24. D. G. Li, G. S. Zhou, J. Zhang and M. S. Zheng, *Electrochim. Acta*, **52**, 2146 (2007).
25. A. G. Gad-Allah, H. A. Abd El-Rahman and M. abd El-Galil, *J. Power Sources*, **62**. 51 (1996).
26. A. G. Gad-Allah, H. A. Abd El-Rahman, S. A. Salih and M. abd El-Galil, *J. Appl. Electrochem.*, **22**, 571 (1992).
27. A. J. Bard and L. R. Faulkner, *Electrochemical Methods, Fundamentals and Applications*, 2nd Ed., Ch 10, Wiley (2001).
28. A. Czerwinski, M. Zelazowska, M. Grden, K. Kuc, J. D. Milewski, A. Nowacki, G. Wojcik and M. Kopczyk, *J.*

Power Sources, **85**, 49 (2000).
29. A. G. Gad-Allah, H. A. Abd El-Rahman, S. A. Salih and M. abd El-Galil, *J. Appl. Electrochem.*, **25**, 682 (1995).
30. H. A. Abd El-Rahman, S. A. Salih and A. M. Abd El-Wahab, *J. Electrochem. Scienec and Technology.*, **2**, 76 (2011).
31. V. Lliev and D. Pavlov, *J. Electrochem. Soc.*, **129**, 1393 (1982).
32. J. S. Symanski, B. K. Mahato and K. R. Bullock, *J. Electrochem. Soc.*, **135**, 548 (1988).